

**Search for Neutral Higgs Bosons of the Minimal
Supersymmetric Standard Model in e^+e^- Interactions at
 $\sqrt{s} = 192 - 202$ GeV**

The L3 Collaboration

Abstract

A search for the lightest neutral CP-even and the neutral CP-odd Higgs bosons of the Minimal Supersymmetric Standard Model is performed using 233.2 pb^{-1} of integrated luminosity collected with the L3 detector at LEP at centre-of-mass energies $192 - 202$ GeV. No signal is observed and lower mass limits are given as a function of $\tan\beta$ for two scalar top mixing hypotheses. For $\tan\beta$ greater than 0.8, they are $m_h > 83.4$ GeV and $m_A > 83.8$ GeV at 95% confidence level.

Submitted to *Phys. Lett. B*

1 Introduction

The Minimal Supersymmetric Standard Model (MSSM) [1] requires two Higgs doublets. This gives rise to five Higgs bosons: a charged scalar pair, two neutral CP-even, the lightest of which is called h , and a neutral CP-odd, A . The two most important production mechanisms in e^+e^- collisions are:

$$e^+e^- \rightarrow Z^* \rightarrow hZ \quad (1)$$

$$e^+e^- \rightarrow Z^* \rightarrow hA. \quad (2)$$

The cross section of the process (1) is smaller than that for the similar production of the Higgs boson in the Standard Model. This process is dominant at low values of $\tan\beta$ ($\tan\beta \lesssim 5$), where $\tan\beta$ is the ratio of the two Higgs vacuum expectation values. The pair-production of Higgs bosons (2) takes over at high values of $\tan\beta$.

Previous searches for the h and A bosons were reported by L3 [2] and other experiments [3]. In this paper, we present the results of the search for the h and A bosons using the data collected with the L3 detector [4] at centre-of-mass energies $\sqrt{s} = 191.6 - 201.7$ GeV, corresponding to 233.2 pb^{-1} of total integrated luminosity. The sensitivity to the production of MSSM neutral Higgs bosons is improved by combining the results of these analyses with our previous searches.

2 Data and Monte Carlo Samples

In 1999 the L3 detector collected data at LEP at average centre-of-mass energies $\sqrt{s} = 191.6$ GeV, 195.5 GeV, 199.5 GeV and 201.7 GeV, corresponding to the integrated luminosities 29.7 pb^{-1} , 83.7 pb^{-1} , 82.8 pb^{-1} and 37.0 pb^{-1} respectively.

The cross sections of processes (1) and (2) and the decay branching ratios of h and A are calculated using the HZHA generator [5]. For efficiency studies, Monte Carlo samples of Higgs events are generated using PYTHIA [6] and HZHA. 2000 Monte Carlo events are generated for each mass hypothesis. For hA samples the masses, m_h and m_A , of the h and A bosons range from 50 to 95 GeV in steps of 5 GeV. For hZ samples m_h is chosen in steps of 5 GeV from 50 to 95 GeV and in steps of 1 GeV from 95 to 110 GeV. For the background studies, the following Monte Carlo programs are used: PYTHIA ($e^+e^- \rightarrow q\bar{q}(\gamma)$, $e^+e^- \rightarrow ZZ$ and $e^+e^- \rightarrow Ze^+e^-$), KORALW [7] ($e^+e^- \rightarrow W^+W^-$), KORALZ [8] ($e^+e^- \rightarrow \tau^+\tau^-$). Hadron production in two-photon interactions is simulated with PYTHIA and PHOJET [9]. EXCALIBUR [10] is used for other four fermion final states. The number of simulated background events for the most important background channels is more than 100 times the corresponding number of expected events.

The L3 detector response is simulated using the GEANT program [11], which models the effects of energy loss, multiple scattering and showering in the detector. The GHEISHA program [12] is used to simulate hadronic interactions in the detector. Time dependent inefficiencies are also taken into account.

3 Event Selection

For the hA production, the following decay modes are considered: $hA \rightarrow b\bar{b}b\bar{b}$, $hA \rightarrow b\bar{b}\tau^+\tau^-$ and $hA \rightarrow \tau^+\tau^-b\bar{b}$. In the case of hZ , four event topologies covering approximately 98% of possible final states, are considered: $q\bar{q}q\bar{q}$, $q\bar{q}\nu\bar{\nu}$, $q\bar{q}l^{+1-}$ ($l = e, \mu, \tau$) and $\tau^+\tau^-q\bar{q}$. The searches

in channels with hadronic decays of the h boson are optimised for the dominant $h \rightarrow b\bar{b}$ decay channel. The analyses $q\bar{q}\nu\bar{\nu}$ and $q\bar{q}l^+l^-$ ($l = e, \mu$) are the same as devised for the Standard Model Higgs search [13].

A common selection is applied to both the hA and hZ searches. In the four-jet channel, it mainly reduces the two-photon interaction background while keeping the signal efficiency high, then a neural network is used to build a discriminating variable. In the tau channel, first a selection is devised, then an optimal variable based on a likelihood approach is defined.

3.1 hA $\rightarrow b\bar{b}b\bar{b}$ and hZ $\rightarrow b\bar{b}q\bar{q}$ Selection

The signature of both the hA $\rightarrow b\bar{b}b\bar{b}$ and hZ $\rightarrow b\bar{b}q\bar{q}$ final states is four hadronic jets and the presence of b-hadrons. The dominant backgrounds come from $q\bar{q}(\gamma)$ production and hadronic decays of W and Z pairs.

High multiplicity events are selected and their visible energy, E_{vis} , is required to be greater than $0.6\sqrt{s}$ and less than $1.4\sqrt{s}$. Events with perpendicular imbalance greater than $0.35E_{\text{vis}}$ or with a lepton whose energy exceeds 65 GeV are rejected to suppress semileptonic W pair decays. Initial state radiation events are further suppressed by requiring $P_{\text{mis}}^L/(m_{\text{vis}} - m_Z) < 0.4$, where P_{mis}^L is the longitudinal component of the missing momentum, m_{vis} is the visible mass and m_Z the Z boson mass. The remaining events are then forced into four jets using the DURHAM algorithm [14] and a kinematic fit requiring energy and momentum conservation (4C) is performed. The number of expected and observed events in the data, together with the signal efficiencies for the selection cuts are listed in Table 1.

After the selection, discriminating variables are combined into a feed forward neural network [15], with one hidden layer and three output nodes. The inputs include the probability that the jets contain b-quarks [16], hereafter termed B_{Tag} , event shape variables and mass information. The information on the event shape includes the event sphericity, the value of the DURHAM jet resolution parameter for which the event is resolved from three to four jets, the longitudinal component of the missing momentum and the event thrust. The mass information is summarised in a χ^2 variable defined as:

$$\chi^2(m_X, m_h) = (\Sigma_{ij}^{\text{min}} - (m_X + m_h))^2 w_\Sigma + (\Delta_{ij}^{\text{min}} - |m_X - m_h|)^2 w_\Delta, \quad (3)$$

where m_X is either m_Z or m_A . The pairing used gives the minimum value for the difference squared $(\Delta_{ij} - |m_X - m_h|)^2$ between the measured and expected dijet mass differences; Σ_{ij}^{min} is the corresponding sum of the dijet masses. The weights, w_Σ and w_Δ , are derived from the mass resolutions, and their ratio is 3/5. In this way, the shape of the neural network output is made almost independent of the mass hypothesis. The polar angle of the Higgs boson, Θ , is also used as input for the hA analysis. It gives additional separation between the hA signal and W^+W^- background, due to the different spins of the W and the Higgs bosons. The distributions of the discriminating input variables are shown in Figure 1.

The Neural Network has three output variables which correspond to the signal, O_{Higgs} , the $q\bar{q}(\gamma)$ final state, O_{qq} , and the W^+W^- final state hypotheses, O_{WW} . The discriminating variable is then obtained from the combination $NN = O_{\text{Higgs}} \times (1 - O_{qq}) \times (1 - O_{WW})$. Two different neural networks are used for the hA and hZ analyses, and the events are classified as hA or hZ according to the largest value of the discriminating variable. The neural network for the hZ is optimised for $m_h = 100$ GeV at $\sqrt{s} = 192-196$ GeV and $m_h = 105$ GeV at $\sqrt{s} = 200-202$ GeV. For the hA search, the neural network is optimised for $m_h = m_A = 85$ GeV. Examples of the discriminating variable distributions of the two analyses are shown in Figure 2. Good agreement

is observed between the data and the expected background. An independent analysis based on a likelihood approach [17] validates the present results.

The highest signal sensitivity region corresponds to large values of NN . For illustrative purposes, in Table 1 we report the number of the observed and expected events selected after the cuts $NN > 0.9$ for the hA analysis, and $NN > 0.5$ for the hZ analysis. The mass distributions for the hA search after the cut $NN > 0.9$ is shown in Figure 3a.

Cut	192 GeV			196 GeV		
	Selection	$NN_{\text{hA}} > 0.9$	$NN_{\text{hZ}} > 0.5$	Selection	$NN_{\text{hA}} > 0.9$	$NN_{\text{hZ}} > 0.5$
Data	430	2	4	1186	3	33
MC	433.6	1.0	9.5	1197.5	3.2	26.0
q \bar{q}	201.2	0.4	3.0	531.3	1.2	7.1
W $^+$ W $^-$	217.9	0.2	4.2	622.3	0.7	11.9
ZZ	14.5	0.4	2.3	43.9	1.3	7.0
ε_{hA}	95.0%	42.0%	65.9%	95.0%	42.0%	65.9%
ε_{hZ}	93.7%	12.6%	52.7%	93.7%	12.6%	52.7%
Cut	200 GeV			202 GeV		
	Selection	$NN_{\text{hA}} > 0.9$	$NN_{\text{hZ}} > 0.5$	Selection	$NN_{\text{hA}} > 0.9$	$NN_{\text{hZ}} > 0.5$
Data	1198	2	9	506	1	6
MC	1118.4	2.0	9.1	507.8	1.0	4.8
q \bar{q}	478.3	0.7	2.5	215.0	0.3	1.5
W $^+$ W $^-$	595.4	0.3	3.3	271.8	0.2	1.7
ZZ	44.7	1.0	3.3	21.0	0.5	1.6
ε_{hA}	94.1%	37.9%	37.9%	95.9%	38.3%	40.4%
ε_{hZ}	91.0%	5.7%	40.9%	92.3%	5.0%	36.3%

Table 1: Number of events observed and expected in the four-jet channels, after the selection and after cuts on the discriminating variables, NN_{hA} and NN_{hZ} . The hA signal efficiencies are quoted for $m_{\text{A}} = m_{\text{h}} = 85$ GeV. The hZ signal efficiencies correspond to $m_{\text{h}} = 100$ GeV at $\sqrt{s} = 192 - 196$ GeV and $m_{\text{h}} = 105$ GeV at $\sqrt{s} = 200 - 202$ GeV.

3.2 hA \rightarrow b \bar{b} $\tau^+\tau^-$, hZ \rightarrow b \bar{b} $\tau^+\tau^-$ and hZ \rightarrow $\tau^+\tau^-$ q \bar{q} Selections

The signatures of hA \rightarrow b \bar{b} $\tau^+\tau^-$ ¹⁾, hZ \rightarrow b \bar{b} $\tau^+\tau^-$ or hZ \rightarrow $\tau^+\tau^-$ q \bar{q} events are a pair of taus accompanied by two hadronic jets. For each of the channels hA and hZ an analysis is optimised based either on the tau identification or on the event topology by requiring four jets with two of them being narrow and of low multiplicity. The main background results from W-pair decays containing taus.

The hZ analysis is similar to the one described in detail in Reference 18. The hA selection is optimised for lower Higgs masses by omitting the cuts on the opening angles of the jets and tau pairs and on the invariant mass of the tau pair, $m_{\tau\tau}$. The invariant mass of the hadronic jets, m_{qq} , must be between 5 GeV and 125 GeV. The ratio of the sum of the energies of the tau decay products over the sum of the energies of the jets is required to be less than one and the value of the missing momentum vector in the rest frame of the Higgs must be less than

¹⁾Both the decay modes (h \rightarrow b \bar{b} , A \rightarrow $\tau^+\tau^-$) and (h \rightarrow $\tau^+\tau^-$, A \rightarrow b \bar{b}) are considered.

40 GeV. Finally, the cosine of the polar angle of the Higgs boson, $|\cos \Theta|$, has to be less than 0.8. The number of events observed, the number expected from background processes, and the signal efficiency for the two selections are listed in Table 2.

For each event class j (ZZ, W^+W^- , $q\bar{q}$, Ze^+e^- , hA, hZ), a probability function, f_j^i , is constructed, where i denotes the variables considered. These are the B_{Tag} for each hadronic jet, $m_{q\bar{q}}$ and $m_{\tau\tau}$. They are presented in Figure 4. The probability, p_j^i , of an event to belong to class j , based on the value of the variable i , is then defined as

$$p_j^i = \frac{f_j^i}{\sum_k f_k^i}. \quad (4)$$

Finally, the probabilities for the individual variables are combined by calculating the likelihood that the event belongs to the either signal class:

$$F_{\text{hA}} = \frac{\prod_i p_{\text{hA}}^i}{\sum_k \prod_i p_k^i} \quad \text{and} \quad F_{\text{hZ}} = \frac{\prod_i p_{\text{hZ}}^i}{\sum_k \prod_i p_k^i}. \quad (5)$$

Events retained by both the hA and the hZ selections, are classified according to highest value of the likelihood, as hA or hZ candidates. An example of the distribution of the discriminating variable for the hA search is shown in Figure 5. Good agreement between the observed data and the expected background is found. The mass distribution for the hA search after an additional cut on the B_{Tag} is shown in Figure 3b.

	192 GeV		196 GeV		200 GeV		202 GeV	
	hA	hZ	hA	hZ	hA	hZ	hA	hZ
Data	2	2	6	7	5	7	3	3
MC	2.6	3.0	7.3	8.4	7.2	7.6	3.2	3.4
$e^+e^- \rightarrow q\bar{q}$	0.3	0.5	0.8	1.4	0.9	0.8	0.4	0.3
$e^+e^- \rightarrow W^+W^-$	1.8	1.8	5.0	5.0	4.6	4.7	2.0	2.1
$e^+e^- \rightarrow ZZ$	0.5	0.6	1.4	1.7	1.6	1.8	0.7	0.8
$e^+e^- \rightarrow Ze^+e^-$	0.0	0.1	0.1	0.2	0.1	0.3	0.0	0.1
$\varepsilon(\text{hA} \rightarrow \text{bb}\tau^+\tau^-)$	36%	36%	36%	36%	33%	34%	33%	34%
$\varepsilon(\text{hZ} \rightarrow \text{bb}\tau^+\tau^-)$	21%	29%	21%	29%	17%	29%	17%	29%
$\varepsilon(\text{hZ} \rightarrow \tau^+\tau^-q\bar{q})$	20%	31%	20%	31%	20%	29%	20%	29%

Table 2: Number of events observed and expected in the tau selection. Efficiencies for the hA signal are quoted for $m_A = m_h = 85$ GeV. For the hZ signal, they are quoted for $m_h = 100$ GeV at $\sqrt{s} = 192 - 196$ GeV and for $m_h = 105$ GeV at $\sqrt{s} = 200 - 202$ GeV.

4 Results and Interpretation

A good agreement between data and expected background, both in the total number of events and in the shape of the distributions, is observed in all the channels analysed. The mass distributions of the events in the highest sensitivity region are not compatible with a signal for any mass hypothesis. Therefore no evidence of the production of the h and A bosons is found.

The results of the search for the hA and the hZ production are interpreted in the framework of the constrained MSSM (CMSSM) assuming unification of the scalar fermion masses, unification of the gaugino masses and unification of the trilinear Higgs-fermion couplings at the GUT scale. This choice has little impact on the phenomenology of the Higgs bosons but reduces significantly the number of free parameters. The remaining free parameters are $\tan\beta$, m_A , the gaugino mass parameter, M_2 , the universal scalar fermion mass, m_0 , the common scalar quark trilinear coupling, A , and the Higgs mixing parameter, μ .

Two benchmark scenarios [19] are considered. In the first one, termed “maximal mixing”, the CMSSM parameters are chosen such that m_h acquires its maximal value for any given value of m_A and $\tan\beta$. The second scenario corresponds to vanishing mixing in the scalar top sector and is referred to as “minimal mixing”.

The CMSSM parameters are chosen as follows: $m_0 = 1$ TeV, $\mu = -200$ GeV, $M_2 = 200$ GeV. The mass of the top quark is fixed to 175 GeV. The maximal mixing scenario is realised at $X_t = A - \mu \cot\beta = \sqrt{6}$ TeV, where X_t is the parameter which controls the mixing in the scalar top sector. The minimal mixing corresponds to $X_t = 0$. Keeping these values fixed, a scan over the two remaining independent parameters, $\tan\beta$ and m_A , is performed in each mixing scheme in the ranges: $0.5 \leq \tan\beta \leq 30$ and $10 \text{ GeV} \leq m_A \leq 1 \text{ TeV}$.

To set exclusion limits on the CMSSM parameters, the confidence level, CL, that the expected signal is absent in the data, is calculated [20] for each point $(\tan\beta, m_A)$ of the scan. The full distributions of the discriminating variables, NN and F , are used in this calculation.

Systematic and statistical uncertainties on the signal and background are evaluated using the same procedure as in the Standard Model Higgs search [13]. The main sources of systematic uncertainties are detector resolution, selection procedures, theoretical uncertainties and Monte Carlo statistics. The overall systematic uncertainties are estimated to be 4% on the predictions for the expected signal and 10% for the background events. Bins of the final variables with a signal-over-background ratio in the Monte Carlo of less than 0.05 are not considered in the calculation of the CL. This cut is chosen to minimise the effect of systematic uncertainties on the average CL as calculated from a large set of Monte Carlo experiments.

The results of the MSSM Higgs search at lower \sqrt{s} [2] are combined with those presented in this paper. Figure 6 shows the region of the $(\tan\beta, m_h)$ plane and $(\tan\beta, m_A)$ plane excluded by L3 for the maximal mixing and minimal mixing scenarios.

For the CMSSM parameters considered and assuming $\tan\beta$ greater than 0.8, this results in lower mass limits at the 95% CL of:

$$m_h > 83.4 \text{ GeV}, \quad m_A > 83.8 \text{ GeV},$$

which compare to the median expected limits in the absence of a signal of $m_h > 85.6$ GeV and $m_A > 85.7$ GeV.

The exclusion plots for the minimal mixing scenario present a small unexcluded area in the low $\tan\beta$ region at low values of m_A where the decay $h \rightarrow AA$ is allowed but is not investigated among the signatures described above.

For $0.8 < \tan\beta < 1.8$ values of m_A up to 1 TeV are ruled out for any mixing scenario allowing to exclude this $\tan\beta$ region in the CMSSM, for the top mass $\lesssim 175$ GeV.

5 Acknowledgements

We acknowledge the efforts of the engineers and technicians who have participated in the construction and maintenance of L3 and express our gratitude to the CERN accelerator divisions

for the superb performance of LEP.

References

- [1] H. P. Nilles, Phys. Rep. **110** (1984) 1; H. E. Haber and G. L. Kane, Phys. Rep. **117** (1985) 75; R. Barbieri, Riv. Nuovo Cim. **11 n°4** (1988) 1
- [2] L3 Collaboration, M. Acciarri *et al.*, Phys. Lett. **B 471** (1999) 321
- [3] OPAL Collaboration, G. Abbiendi *et al.*, Eur. Phys. **C 12** (2000) 567; ALEPH Collaboration, R. Barate *et al.*, Preprint CERN-EP/2000-131 (2000); DELPHI Collaboration, P. Abreu *et al.*, Preprint CERN-EP/2000-038 (2000)
- [4] L3 Collaboration, B. Adeva *et al.* Nucl. Inst. Meth. **A 289** (1990) 35; J. A. Bakken *et al.*, Nucl. Inst. Meth. **A 275** (1989) 81; O. Adriani *et al.*, Nucl. Inst. Meth. **A 302** (1991) 53; B. Adeva *et al.*, Nucl. Inst. Meth. **A 323** (1992) 109; K. Deiters *et al.*, Nucl. Inst. Meth. **A 323** (1992) 162; M. Chemarin *et al.*, Nucl. Inst. Meth. **A 349** (1994) 345; M. Acciarri *et al.*, Nucl. Inst. Meth. **A 351** (1994) 300; G. Basti *et al.*, Nucl. Inst. Meth. **A 374** (1996) 293; A. Adam *et al.*, Nucl. Inst. Meth. **A 383** (1996) 342
- [5] P. Janot, “The HZHA Generator” in *Physics at LEP2*, eds. G. Altarelli *et al.*, CERN 96-01 (1996), vol. 2, p. 309. Version 3, released in December 1999, <http://alephwww.cern.ch/~janot/Generators.html>
- [6] PYTHIA version 5.722 is used; T. Sjöstrand, Preprint CERN-TH/93-7112 (1993), revised 1995; T. Sjöstrand, Comp. Phys. Comm. **82** (1994) 74
- [7] KORALW version 1.33 is used; M. Skrzypek *et al.*, Comp. Phys. Comm. **94** (1996) 216; M. Skrzypek *et al.*, Phys. Lett. **B 372** (1996) 289
- [8] KORALZ version 4.03 is used; S. Jadach and B. F. L. Ward and Z. Wąs, Comp. Phys. Comm. **79** (1994) 503
- [9] PHOJET version 1.05 is used; R. Engel, Z. Phys. **C 66** (1995) 203; R. Engel and J. Ranft and S. Roesler, Phys. Rev. **D 52** (1995) 1459
- [10] F. A. Berends and R. Pittau and R. Kleiss, Comp. Phys. Comm. **85** (1995) 437
- [11] GEANT version 3.15 is used; R. Brun *et al.*, Preprint CERN DD/EE/84-1 (1984), revised 1987
- [12] H. Fesefeldt, Report RWTH Aachen PITHA 85/02 (1985)
- [13] L3 Collaboration, M. Acciarri *et al.*, Preprint CERN-EP/2000-146 (2000)
- [14] S. Bethke *et al.*, Nucl. Phys. **B 370** (1992) 310
- [15] L. Lönnblad and C. Peterson and T. Rognvaldsson, Nucl. Phys. **B 349** (1991) 675; C. Peterson *et al.*, Comp. Phys. Comm. **81** (1994) 185
- [16] L3 Collaboration, M. Acciarri *et al.*, Phys. Lett. **B 411** (1997) 373

- [17] L3 Collaboration, M. Acciarri *et al.*, Phys. Lett. **B 436** (1998) 389
- [18] L3 Collaboration, M. Acciarri *et al.*, Phys. Lett. **B 461** (1999) 376
- [19] M. Carena *et al.*, Preprint hep-ph/9912223 (1999)
- [20] A. Read, “Modified Frequentist Analysis of Search Results (The CLs Method)” in *Workshop on Confidence Limits*, eds. F. James *et al.*, CERN 2000-05, p. 81
- [21] OPAL Collaboration, G. Alexander *et al.*, Z. Phys. **C 73** (1997) 189 .

The L3 Collaboration:

M.Acciarri;²⁶ P.Achard;¹⁹ O.Adriani;¹⁶ M.Aguilar-Benitez;²⁵ J.Alcaraz;²⁵ G.Alemanni;²² J.Allaby;¹⁷ A.Aloisio;²⁸ M.G.Alvigi;²⁸ G.Ambrosi;¹⁹ H.Anderhub;⁴⁸ V.P.Andreev;^{6,36} T.Angelescu;¹² F.Anselmo;⁹ A.Arefiev;²⁷ T.Azemoon;³ T.Aziz;¹⁰ P.Bagnaia;³⁵ A.Bajo;²⁵ L.Baksay;⁴³ A.Balandras;⁴ S.V.Baldew;² S.Banerjee;¹⁰ Sw.Banerjee;⁴ A.Barczyk;^{48,46} R.Barillère;¹⁷ P.Bartalini;²² M.Basile;⁹ N.Batalova;⁴⁵ R.Battiston;³² A.Bay;²² F.Becattini;¹⁶ U.Becker;¹⁴ F.Behner;⁴⁸ L.Bellucci;¹⁶ R.Berbeco;³ J.Berdugo;²⁵ P.Berges;¹⁴ B.Bertucci;³² B.L.Betev;⁴⁸ S.Bhattacharya;¹⁰ M.Biasini;³² A.Biland;⁴⁸ J.J.Blaising;⁴ S.C.Blyth;³³ G.J.Bobbink;² A.Böhm;¹ L.Boldizsar;¹³ B.Borgia;³⁵ D.Bourilkov;⁴⁸ M.Bourquin;¹⁹ S.Braccini;¹⁹ J.G.Branson;⁴⁰ F.Brochu;⁴ A.Buffini;¹⁶ A.Buijs;⁴⁴ J.D.Burger;¹⁴ W.J.Burger;³² X.D.Cai;¹⁴ M.Capell;¹⁴ G.Cara Romeo;⁹ G.Carlino;²⁸ A.M.Cartacci;¹⁶ J.Casaus;²⁵ G.Castellini;¹⁶ F.Cavallari;³⁵ N.Cavallo;³⁷ C.Cecchi;³² M.Cerrada;²⁵ F.Cesaroni;²³ M.Chamizo;¹⁹ Y.H.Chang;⁵⁰ U.K.Chaturvedi;¹⁸ M.Chemarin;²⁴ A.Chen;⁵⁰ G.Chen;⁷ G.M.Chen;⁷ H.F.Chen;²⁰ H.S.Chen;⁷ G.Chiefari;²⁸ L.Cifarelli;³⁹ F.Cindolo;⁹ C.Civinini;¹⁶ I.Clare;¹⁴ R.Clare;³⁸ G.Coignet;⁴ N.Colino;²⁵ S.Costantini;⁵ F.Cotorobai;¹² B.de la Cruz;²⁵ A.Csilling;¹³ S.Cucciarelli;³² T.S.Dai;¹⁴ J.A.van Dalen;³⁰ R.D'Alessandro;¹⁶ R.de Asmundis;²⁸ P.Dégion;¹⁹ A.Degré;⁴ K.Deiters;⁴⁶ D.della Volpe;²⁸ E.Delmeire;¹⁹ P.Denes;³⁴ F.DeNotaristefani;³⁵ A.De Salvo;⁴⁸ M.Diemoz;³⁵ M.Dierckxsens;² D.van Dierendonck;² C.Dionisi;³⁵ M.Dittmar;⁴⁸ A.Dominguez;⁴⁰ A.Doria;²⁸ M.T.Dova;^{18,4} D.Duchesneau;⁴ D.Dufournaud;⁴ P.Duinker;² H.El Mamouni;²⁴ A.Engler;³³ F.J.Eppling;¹⁴ F.C.Erné;¹⁷ A.Ewers;¹ P.Extermann;¹⁹ M.Fabre;⁴⁶ M.A.Falagan;²⁵ S.Falciano;^{35,17} A.Favara;¹⁷ J.Fay;²⁴ O.Fedin;³⁶ M.Felcini;⁴⁸ T.Ferguson;³³ H.Fesefeldt;¹ E.Fiandrini;³² J.H.Field;¹⁹ F.Filthaut;¹⁷ P.H.Fisher;¹⁴ I.Fisk;⁴⁰ G.Forconi;¹⁴ K.Freudenreich;⁴⁸ C.Furetta;²⁶ Yu.Galaktionov;^{27,14} S.N.Ganguli;¹⁰ P.Garcia-Abia;⁵ M.Gataullin;³¹ S.S.Gau;¹¹ S.Gentile;^{35,17} N.Gheordanescu;¹² S.Giagu;³⁵ Z.F.Gong;²⁰ G.Grenier;²⁴ O.Grimm;⁴⁸ M.W.Gruenewald;⁸ M.Guida;³⁹ R.van Gulik;² V.K.Gupta;³⁴ A.Gurtu;¹⁰ L.J.Gutay;⁴⁵ D.Haas;⁵ A.Hasan;²⁹ D.Hatzifotiadou;⁹ T.Hebbeker;⁸ A.Hervé;¹⁷ P.Hidas;¹³ J.Hirschfelder;³³ H.Hofer;⁴⁸ G.Holzner;⁴⁸ H.Hoorani;³³ S.R.Hou;⁵⁰ Y.Hu;³⁰ I.Iashvili;⁴⁷ B.N.Jin;⁷ L.W.Jones;³ P.de Jong;² I.Josa-Mutuberría;²⁵ R.A.Khan;¹⁸ D.Käfer;¹ M.Kaur;^{18,4} M.N.Kienzle-Focacci;¹⁹ D.Kim;³⁵ J.K.Kim;⁴² J.Kirkby;¹⁷ D.Kiss;¹³ W.Kittel;³⁰ A.Klimentov;^{14,27} A.C.König;³⁰ M.Kopal;⁴⁵ A.Kopp;⁴⁷ V.Koutsenko;^{14,27} M.Kräber;⁴⁸ R.W.Kraemer;³³ W.Krenz;¹ A.Krüger;⁴⁷ A.Kunin;^{14,27} P.Ladron de Guevara;²⁵ I.Laktineh;²⁴ G.Landi;¹⁶ M.Lebeau;¹⁷ A.Lebedev;¹⁴ P.Lebrun;²⁴ P.Lecomte;⁴⁸ P.Lecoq;¹⁷ P.Le Coultre;⁴⁸ H.J.Lee;⁸ J.M.Le Goff;¹⁷ R.Leiste;⁴⁷ P.Levtchenko;³⁶ C.Li;²⁰ S.Likhoded;⁴⁷ C.H.Lin;⁵⁰ W.T.Lin;⁵⁰ F.L.Linde;² L.Lista;²⁸ Z.A.Liu;⁷ W.Lohmann;⁴⁷ E.Longo;³⁵ Y.S.Lu;⁷ K.Lübelsmeyer;¹ C.Luci;^{17,35} D.Luckey;¹⁴ L.Lugnier;²⁴ L.Luminari;³⁵ W.Lustermann;⁴⁸ W.G.Ma;²⁰ M.Maity;¹⁰ L.Malgeri;¹⁷ A.Malinin;¹⁷ C.Maia;²⁵ D.Mangeol;³⁰ J.Mans;³⁴ G.Marian;¹⁵ J.P.Martin;²⁴ F.Marzano;³⁵ K.Mazumdar;¹⁰ R.R.McNeil;⁶ S.Mele;¹⁷ L.Merola;²⁸ M.Meschini;¹⁶ W.J.Metzger;³⁰ M.von der Mey;¹ A.Mihul;¹² H.Milcent;¹⁷ G.Mirabelli;³ J.Mnich;¹ G.B.Mohanty;¹⁰ T.Moulik;¹⁰ G.S.Muanza;²⁴ A.J.M.Muijs;² B.Musicar;⁴⁰ M.Musy;³⁵ M.Napolitano;²⁸ F.Nessi-Tedaldi;⁴⁸ H.Newman;³¹ T.Niessen;¹ A.Nisati;³⁵ H.Nowak;⁴⁷ R.Ofierzynski;⁴⁸ G.Organtini;³⁵ A.Oulianov;²⁷ C.Palomares;²⁵ D.Pandoulas;¹ S.Paoletti;^{35,17} P.Paolucci;²⁸ R.Paramatti;³⁵ H.K.Park;³³ I.H.Park;⁴² G.Passaleva;¹⁷ S.Patricelli;²⁸ T.Paul;¹¹ M.Pauluzzi;³² C.Paus;¹⁷ F.Pauss;⁴⁸ M.Pedace;³⁵ S.Pensotti;²⁶ D.Perret-Gallix;⁴ B.Petersen;³⁰ D.Piccolo;²⁸ F.Pierella;⁹ M.Pieri;¹⁶ P.A.Piroué;³⁴ E.Pistoiesi;²⁶ V.Plyaskin;²⁷ M.Pohl;¹⁹ V.Pojidaev;^{27,16} H.Postema;¹⁴ J.Pothier;¹⁷ D.O.Prokofiev;⁴⁵ D.Prokofiev;³⁶ J.Quartieri;³⁹ G.Rahal-Callot;^{48,17} M.A.Rahaman;¹⁰ P.Raics;¹⁵ N.Raja;¹⁰ R.Ramelli;⁴⁸ P.G.Rancoita;²⁶ R.Ranieri;¹⁶ A.Raspereza;⁴⁷ G.Raven;⁴⁰ P.Razis;²⁹ D.Ren;⁴⁸ M.Rescigno;³⁵ S.Reucroft;¹¹ S.Riemann;⁴⁷ K.Riles;³ J.Rodin;⁴³ B.P.Roe;³ L.Romero;²⁵ A.Rosca;⁸ S.Rosier-Lees;⁴ S.Roth;¹ C.Rosenbleck;¹ B.Roux;³⁰ J.A.Rubio;¹⁷ G.Ruggiero;¹⁶ H.Rykaczewski;⁴⁸ S.Saremi;⁶ S.Sarkar;³⁵ J.Salicio;¹⁷ E.Sanchez;¹⁷ M.P.Sanders;³⁰ C.Schäfer;¹⁷ V.Schegelsky;³⁶ S.Schmidt-Kaerst;¹ D.Schmitz;¹ H.Schopper;⁴⁹ D.J.Schotanus;³⁰ G.Schwering;¹ C.Sciacca;²⁸ A.Seganti;⁹ L.Servoli;³² S.Shevchenko;³¹ N.Shivarov;⁴¹ V.Shoutko;²⁷ E.Shumilov;²⁷ A.Shvorob;³¹ T.Siedenburger;¹ D.Son;⁴² B.Smith;³³ P.Spillantini;¹⁶ M.Steuer;¹⁴ D.P.Stickland;³⁴ A.Stone;⁶ B.Stoyanov;⁴¹ A.Straessner;¹ K.Sudhakar;¹⁰ G.Sultanov;¹⁸ L.Z.Sun;²⁰ S.Sushkov;⁸ H.Suter;⁴⁸ J.D.Swain;¹⁸ Z.Szillasi;^{43,4} T.Szutaricskai;^{43,4} X.W.Tang;⁷ L.Tauscher;⁵ L.Taylor;¹¹ B.Tellili;²⁴ D.Teyssier;²⁴ C.Timmermans;³⁰ Samuel C.C.Ting;¹⁴ S.M.Ting;¹⁴ S.C.Tonwar;¹⁰ J.Tóth;¹³ C.Tully;¹⁷ K.L.Tung;⁷ Y.Uchida;¹⁴ J.Ulbricht;⁴⁸ E.Valente;³⁵ G.Vesztergombi;¹³ I.Vetlitsky;²⁷ D.Vicinanza;³⁹ G.Viertel;⁴⁸ S.Villa;¹¹ M.Vivargent;⁴ S.Vlachos;⁵ I.Vodopianov;³⁶ H.Vogel;³³ H.Vogt;⁴⁷ I.Vorobiev;³³ A.A.Vorobyov;³⁶ A.Vorvolakos;²⁹ M.Wadhwa;⁵ W.Wallraff;¹ M.Wang;¹⁴ X.L.Wang;²⁰ Z.M.Wang;²⁰ A.Weber;¹ M.Weber;¹ P.Wienemann;¹ H.Wilkens;³⁰ S.X.Wu;¹⁴ S.Wynhoff;¹⁷ L.Xia;³¹ Z.Z.Xu;²⁰ J.Yamamoto;³ B.Z.Yang;²⁰ C.G.Yang;⁷ H.J.Yang;⁷ M.Yang;⁷ J.B.Ye;²⁰ S.C.Yeh;⁵¹ An.Zalite;³⁶ Yu.Zalite;³⁶ Z.P.Zhang;²⁰ G.Y.Zhu;⁷ R.Y.Zhu;³¹ A.Zichichi;^{9,17,18} G.Zilizi;^{43,4} B.Zimmermann;⁴⁸ M.Zöller;¹

- 1 I. Physikalisches Institut, RWTH, D-52056 Aachen, FRG[§]
III. Physikalisches Institut, RWTH, D-52056 Aachen, FRG[§]
 - 2 National Institute for High Energy Physics, NIKHEF, and University of Amsterdam, NL-1009 DB Amsterdam, The Netherlands
 - 3 University of Michigan, Ann Arbor, MI 48109, USA
 - 4 Laboratoire d'Annecy-le-Vieux de Physique des Particules, LAPP, IN2P3-CNRS, BP 110, F-74941 Annecy-le-Vieux CEDEX, France
 - 5 Institute of Physics, University of Basel, CH-4056 Basel, Switzerland
 - 6 Louisiana State University, Baton Rouge, LA 70803, USA
 - 7 Institute of High Energy Physics, IHEP, 100039 Beijing, China[△]
 - 8 Humboldt University, D-10099 Berlin, FRG[§]
 - 9 University of Bologna and INFN-Sezione di Bologna, I-40126 Bologna, Italy
 - 10 Tata Institute of Fundamental Research, Bombay 400 005, India
 - 11 Northeastern University, Boston, MA 02115, USA
 - 12 Institute of Atomic Physics and University of Bucharest, R-76900 Bucharest, Romania
 - 13 Central Research Institute for Physics of the Hungarian Academy of Sciences, H-1525 Budapest 114, Hungary[‡]
 - 14 Massachusetts Institute of Technology, Cambridge, MA 02139, USA
 - 15 KLTE-ATOMKI, H-4010 Debrecen, Hungary[¶]
 - 16 INFN Sezione di Firenze and University of Florence, I-50125 Florence, Italy
 - 17 European Laboratory for Particle Physics, CERN, CH-1211 Geneva 23, Switzerland
 - 18 World Laboratory, FBLJA Project, CH-1211 Geneva 23, Switzerland
 - 19 University of Geneva, CH-1211 Geneva 4, Switzerland
 - 20 Chinese University of Science and Technology, USTC, Hefei, Anhui 230 029, China[△]
 - 22 University of Lausanne, CH-1015 Lausanne, Switzerland
 - 23 INFN-Sezione di Lecce and Università Degli Studi di Lecce, I-73100 Lecce, Italy
 - 24 Institut de Physique Nucléaire de Lyon, IN2P3-CNRS, Université Claude Bernard, F-69622 Villeurbanne, France
 - 25 Centro de Investigaciones Energéticas, Medioambientales y Tecnológicas, CIEMAT, E-28040 Madrid, Spain^b
 - 26 INFN-Sezione di Milano, I-20133 Milan, Italy
 - 27 Institute of Theoretical and Experimental Physics, ITEP, Moscow, Russia
 - 28 INFN-Sezione di Napoli and University of Naples, I-80125 Naples, Italy
 - 29 Department of Natural Sciences, University of Cyprus, Nicosia, Cyprus
 - 30 University of Nijmegen and NIKHEF, NL-6525 ED Nijmegen, The Netherlands
 - 31 California Institute of Technology, Pasadena, CA 91125, USA
 - 32 INFN-Sezione di Perugia and Università Degli Studi di Perugia, I-06100 Perugia, Italy
 - 33 Carnegie Mellon University, Pittsburgh, PA 15213, USA
 - 34 Princeton University, Princeton, NJ 08544, USA
 - 35 INFN-Sezione di Roma and University of Rome, "La Sapienza", I-00185 Rome, Italy
 - 36 Nuclear Physics Institute, St. Petersburg, Russia
 - 37 INFN-Sezione di Napoli and University of Potenza, I-85100 Potenza, Italy
 - 38 University of California, Riverside, CA 92521, USA
 - 39 University and INFN, Salerno, I-84100 Salerno, Italy
 - 40 University of California, San Diego, CA 92093, USA
 - 41 Bulgarian Academy of Sciences, Central Lab. of Mechatronics and Instrumentation, BU-1113 Sofia, Bulgaria
 - 42 Laboratory of High Energy Physics, Kyungpook National University, 702-701 Taegu, Republic of Korea
 - 43 University of Alabama, Tuscaloosa, AL 35486, USA
 - 44 Utrecht University and NIKHEF, NL-3584 CB Utrecht, The Netherlands
 - 45 Purdue University, West Lafayette, IN 47907, USA
 - 46 Paul Scherrer Institut, PSI, CH-5232 Villigen, Switzerland
 - 47 DESY, D-15738 Zeuthen, FRG
 - 48 Eidgenössische Technische Hochschule, ETH Zürich, CH-8093 Zürich, Switzerland
 - 49 University of Hamburg, D-22761 Hamburg, FRG
 - 50 National Central University, Chung-Li, Taiwan, China
 - 51 Department of Physics, National Tsing Hua University, Taiwan, China
- [§] Supported by the German Bundesministerium für Bildung, Wissenschaft, Forschung und Technologie
[‡] Supported by the Hungarian OTKA fund under contract numbers T019181, F023259 and T024011.
[¶] Also supported by the Hungarian OTKA fund under contract numbers T22238 and T026178.
^b Supported also by the Comisión Interministerial de Ciencia y Tecnología.
[‡] Also supported by CONICET and Universidad Nacional de La Plata, CC 67, 1900 La Plata, Argentina.
[◇] Also supported by Panjab University, Chandigarh-160014, India.
[△] Supported by the National Natural Science Foundation of China.

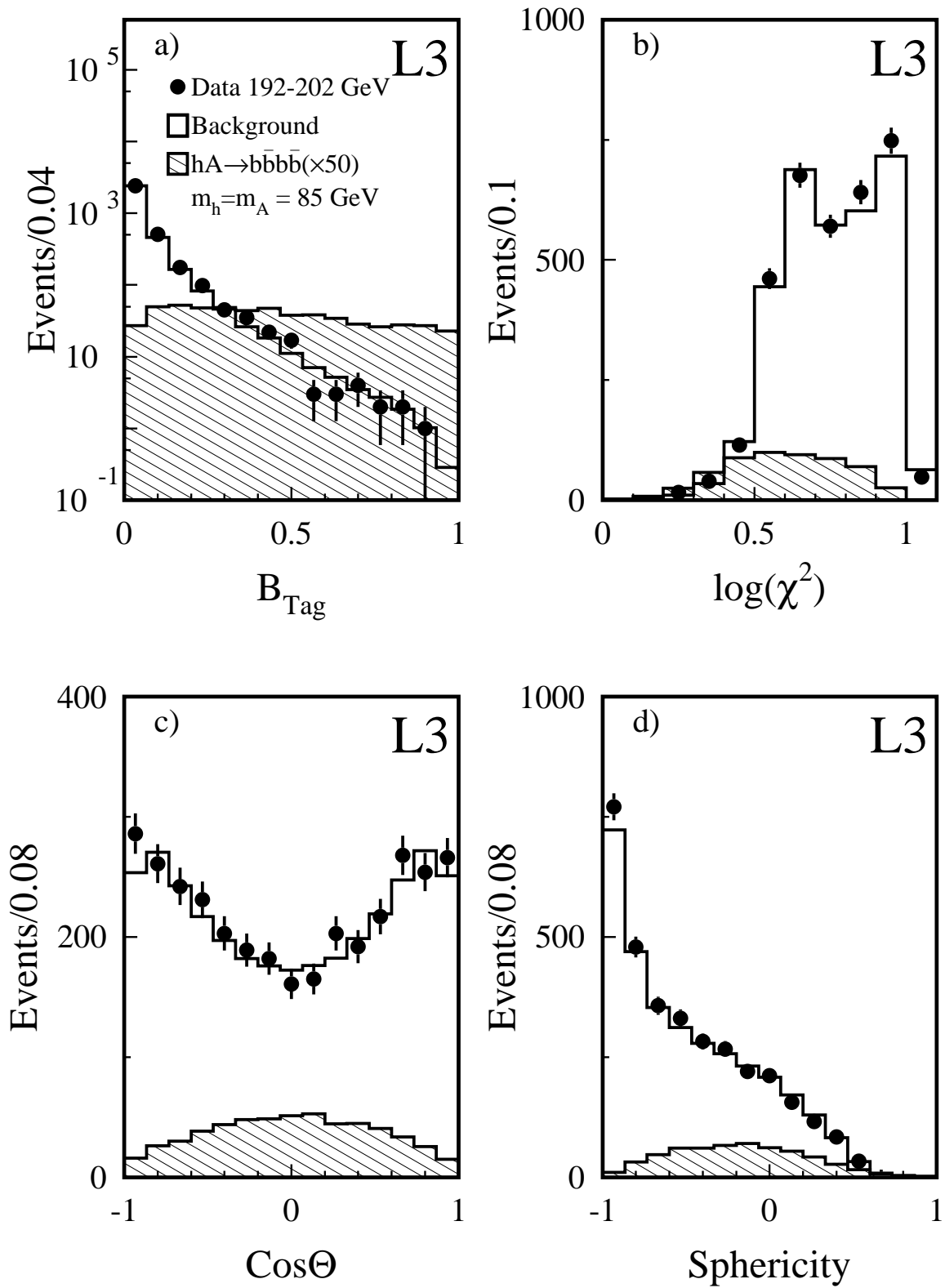


Figure 1: Distributions of a) B_{Tag} , b) logarithm of the χ^2 variable, c) cosine of the polar angle Θ of the Higgs boson and d) sphericity after the four-jet selection. The points represent the data at $\sqrt{s} = 192 - 202 \text{ GeV}$, the open histograms are the expected Standard Model backgrounds, and the hatched histograms are the expected $hA \rightarrow b\bar{b}b\bar{b}$ signal scaled by a factor 50, for $m_h = m_A = 85 \text{ GeV}$ at $\tan\beta = 30$.

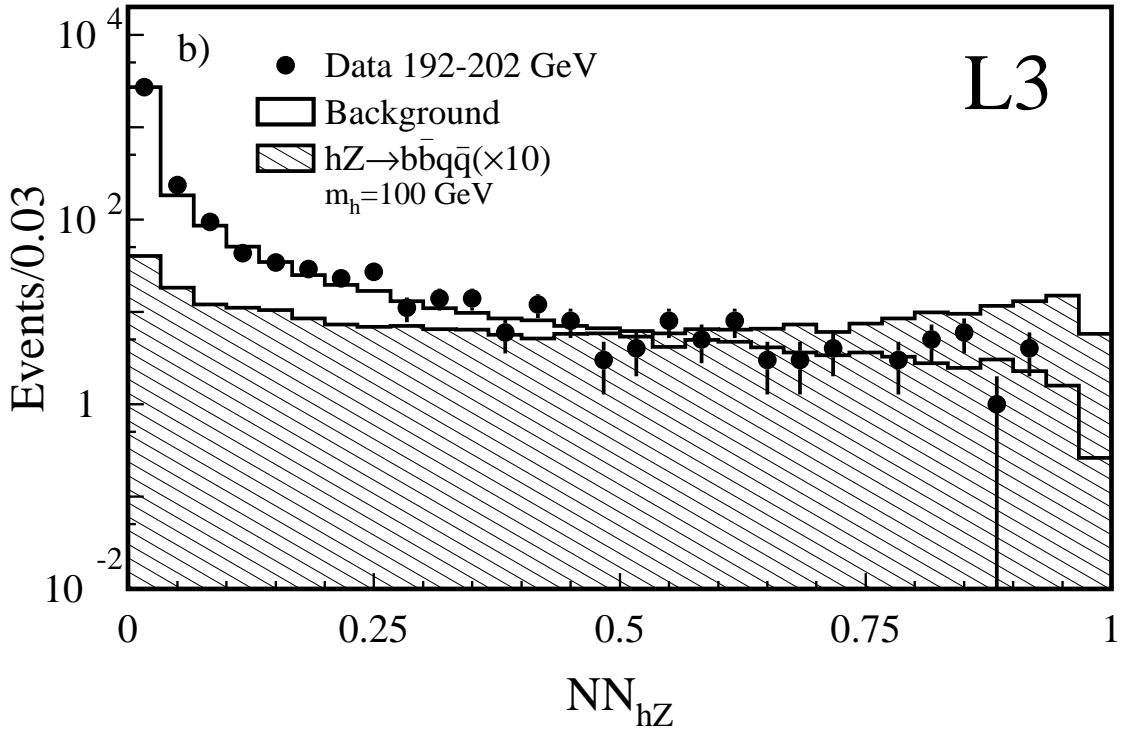
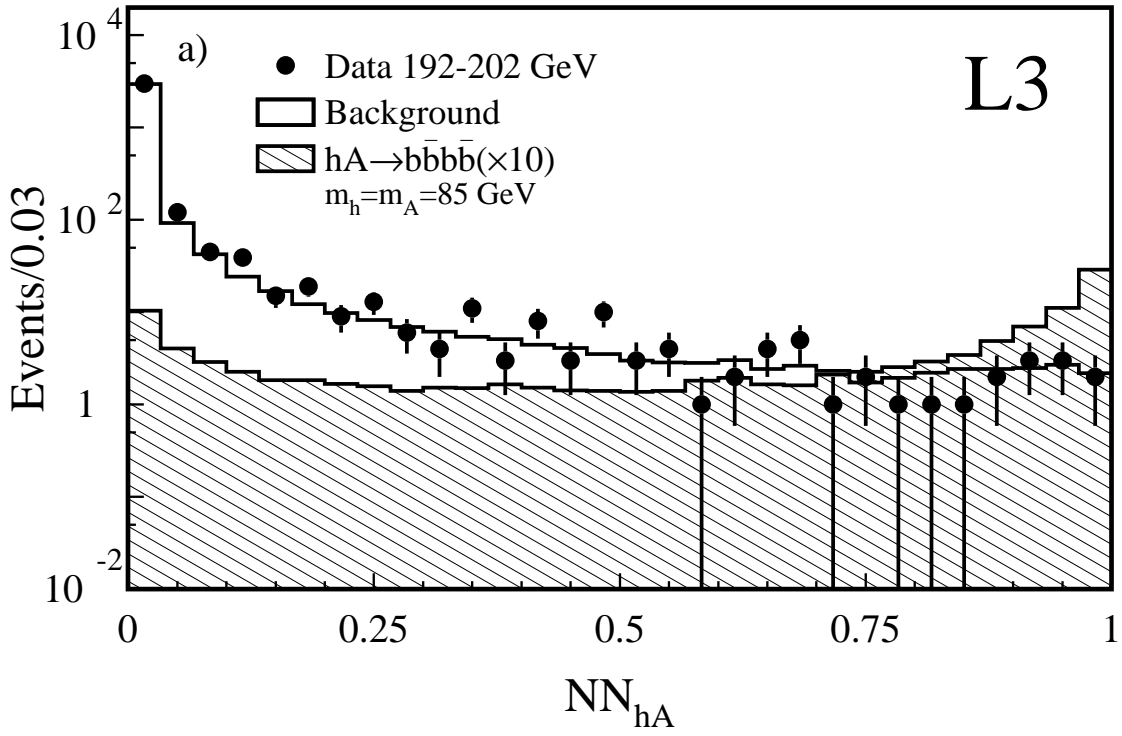


Figure 2: Distributions of the discriminating variable in the four jet channel for a) $hA \rightarrow b\bar{b}b\bar{b}$ and b) $hZ \rightarrow b\bar{b}q\bar{q}$. The points show the data collected at $\sqrt{s} = 192 - 202 \text{ GeV}$, the open histograms are the expected Standard Model backgrounds and the hatched histograms are the expected signals scaled by a factor 10. The discriminating variables are constructed assuming equal mass hypothesis $m_h = m_A = 85 \text{ GeV}$ at $\tan\beta = 30$ in a) and $m_h = 100 \text{ GeV}$ at $\tan\beta = 1$ in b).

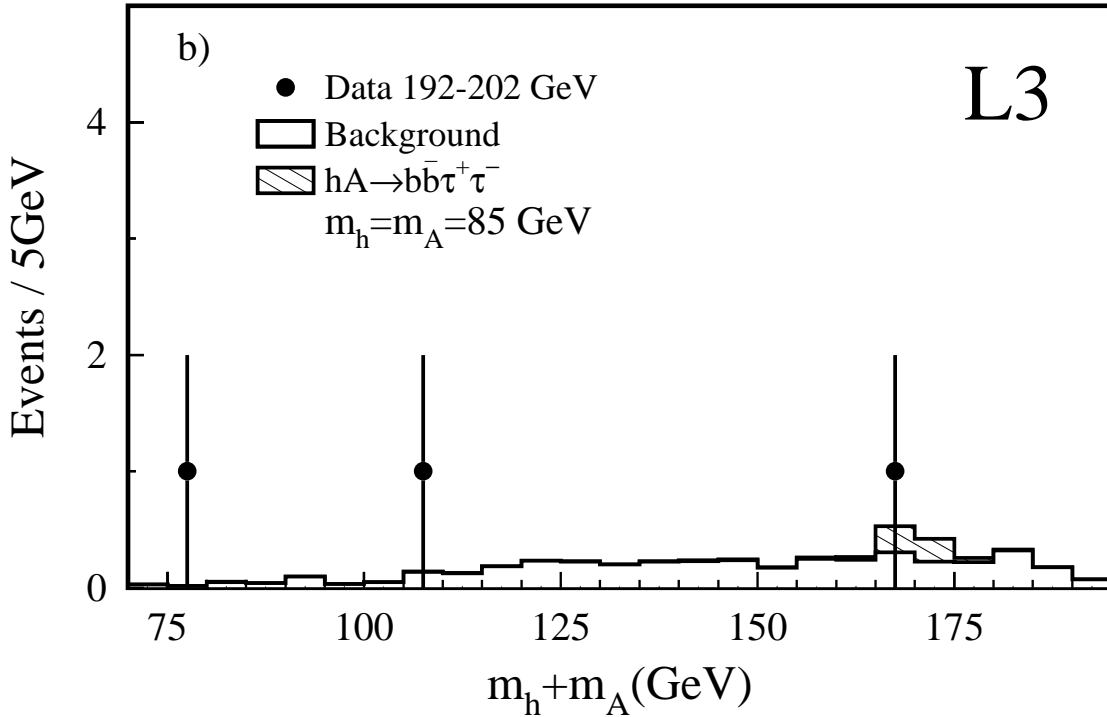
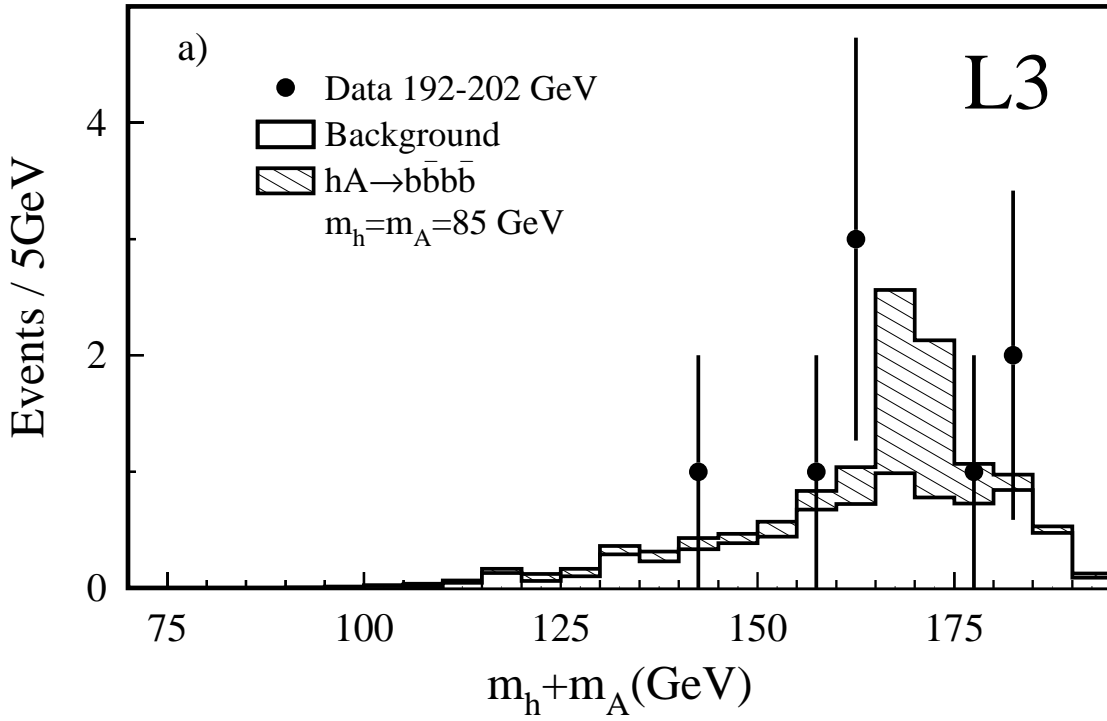


Figure 3: Distributions of a) the sum of the reconstructed dijet masses in the $hA \rightarrow b\bar{b}b\bar{b}$ channel after the cut $NN > 0.9$, b) the sum of the dijet and the ditau masses in the $hA \rightarrow b\bar{b}\tau^+\tau^-$ channel after a cut on the B_{Tag} . The points represent the data collected at $\sqrt{s} = 192-202$ GeV, the open histogram is the expected Standard Model background and the hatched histogram is the expected signal for $m_h = m_A = 85$ GeV at $\tan\beta = 30$.

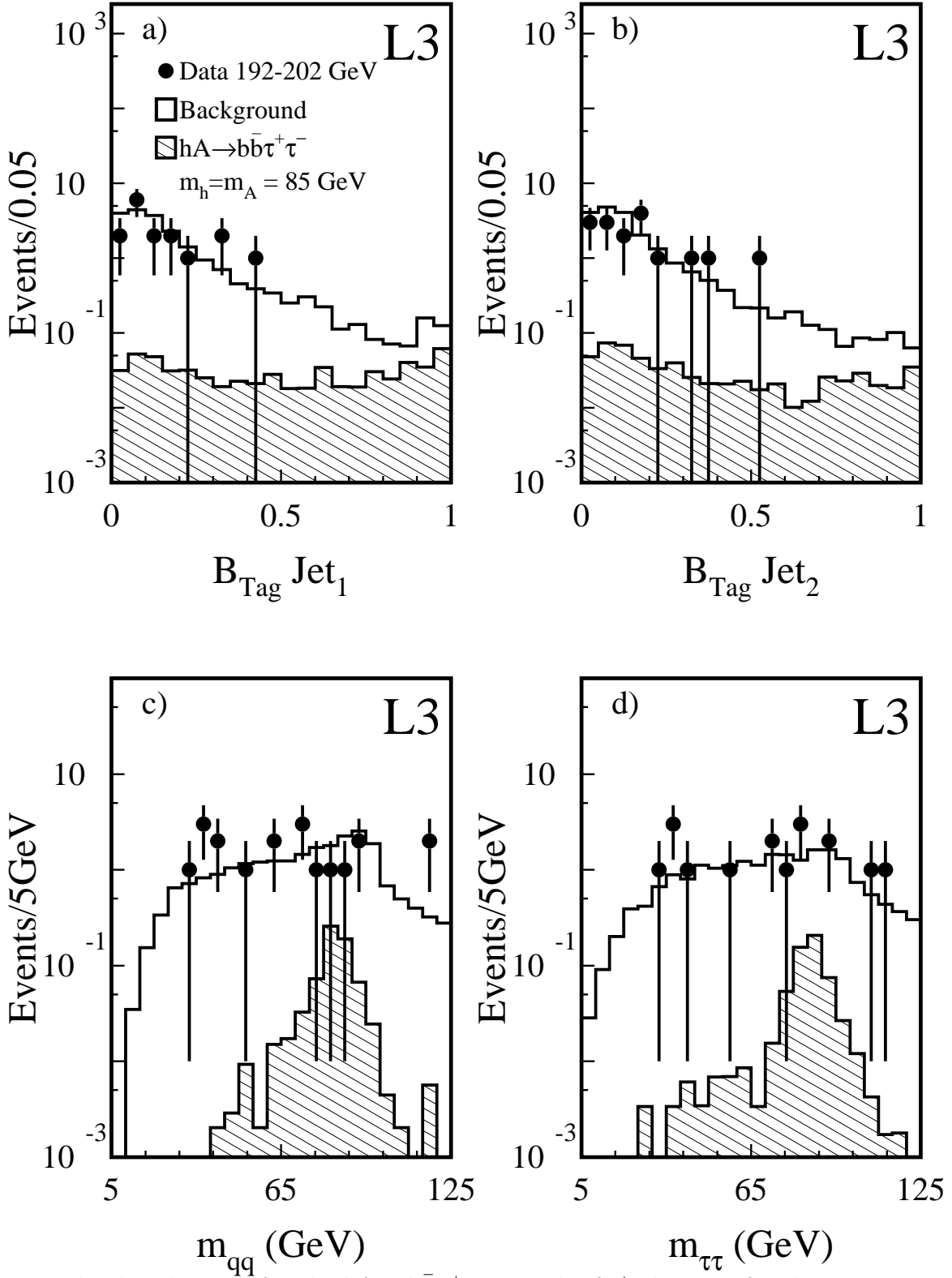


Figure 4: The distributions for the $hA \rightarrow b\bar{b}\tau^+\tau^-$ search of a) the B_{Tag} for the most energetic hadronic jet and b) the least energetic hadronic jet, c) the reconstructed mass for the hadronic system, and d) the reconstructed mass for the leptonic system. The points are the $\sqrt{s} = 192 - 202 \text{ GeV}$ data, the open histograms the expected Standard Model background and the hatched histograms the expected $hA \rightarrow b\bar{b}\tau^+\tau^-$ signal for $m_h = m_A = 85 \text{ GeV}$ at $\tan\beta = 30$.

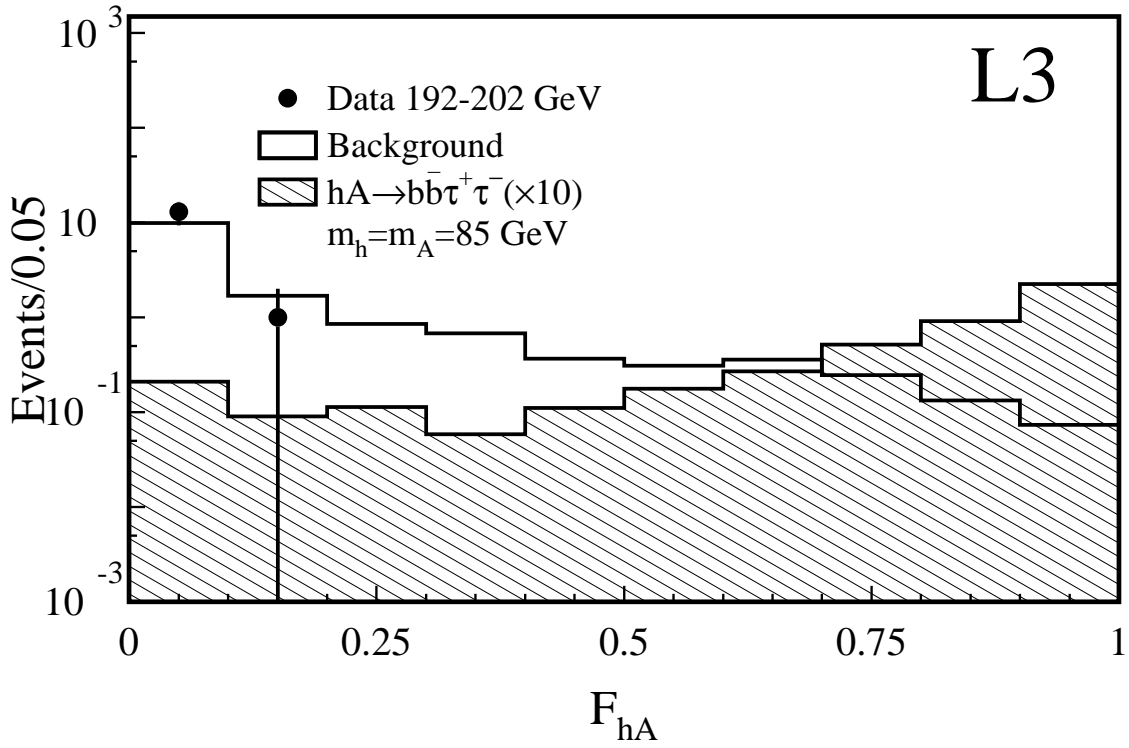


Figure 5: Distribution of the discriminating variable of the $hA \rightarrow b\bar{b}\tau^+\tau^-$ selection in the hypothesis $m_h = m_A = 85$ GeV at $\tan\beta = 30$. The points are the data collected at $\sqrt{s} = 192 - 202$ GeV, the open histogram is the expected Standard Model background and the hatched histogram is the expected signal for the hA search multiplied by a factor 10.

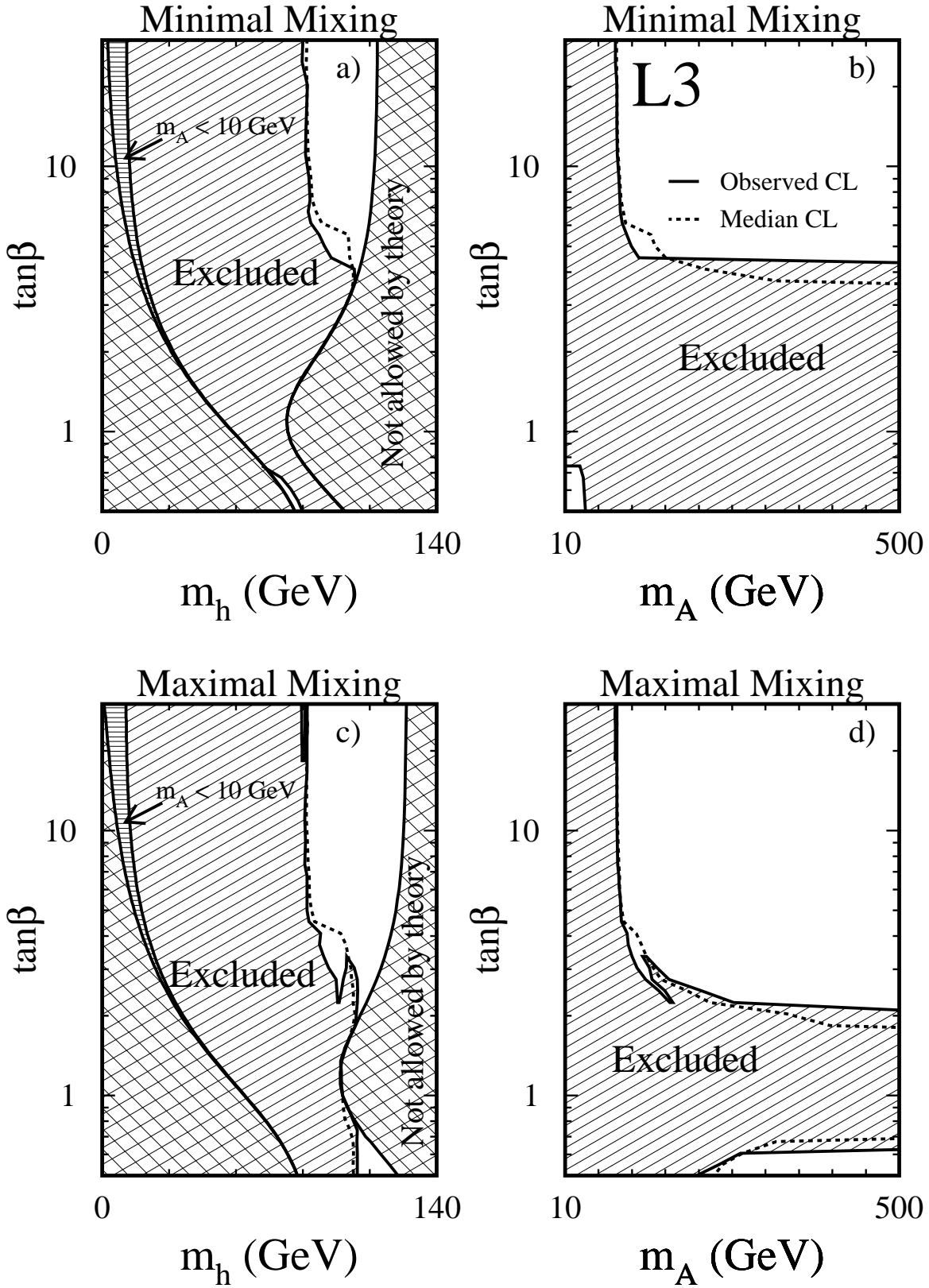


Figure 6: Exclusion plots in the $(\tan\beta, m_h)$ and $(\tan\beta, m_A)$ planes at the 95% CL for the minimal and maximal mixing scenarios. The hatched area represents the exclusion and the crossed area is not allowed by the theory. The horizontal hatched area corresponds to $m_A < 10 \text{ GeV}$ and was previously excluded at LEP [21].